

## Quantum memory and gates using a $\Lambda$ -type quantum emitter coupled to a chiral waveguide

Tao Li,<sup>1</sup> Adam Miranowicz,<sup>1,2,\*</sup> Xuedong Hu,<sup>1,3</sup> Keyu Xia,<sup>1,4,†</sup> and Franco Nori<sup>1,5,‡</sup>

<sup>1</sup>*Theoretical Quantum Physics Laboratory, RIKEN Cluster for Pioneering Research, Wako-shi, Saitama 351-0198, Japan*

<sup>2</sup>*Faculty of Physics, Adam Mickiewicz University, 61-614 Poznań, Poland*

<sup>3</sup>*Department of Physics, University at Buffalo, SUNY, Buffalo, New York 14260-1500, USA*

<sup>4</sup>*College of Engineering and Applied Sciences, Nanjing University, Nanjing 210008, China*

<sup>5</sup>*Physics Department, The University of Michigan, Ann Arbor, Michigan 48109-1040, USA*



(Received 15 March 2018; published 11 June 2018)

By coupling a  $\Lambda$ -type quantum emitter to a chiral waveguide, in which the polarization of a photon is locked to its propagation direction, we propose a controllable photon-emitter interface for quantum networks. We show that this chiral system enables the SWAP gate and a hybrid-entangling gate between the emitter and a flying single photon. It also allows deterministic storage and retrieval of single-photon states with high fidelities and efficiencies. In short, this chirally coupled emitter-photon interface can be a critical building block toward a large-scale quantum network.

DOI: [10.1103/PhysRevA.97.062318](https://doi.org/10.1103/PhysRevA.97.062318)

### I. INTRODUCTION

A quantum network could provide secure information distribution protected by the quantum no-cloning theorem [1–3]. Photons at optical frequencies, which usually interact weakly with their environment, are natural information carriers (a quantum bus) in a quantum network, connecting remote quantum computer nodes [4–7] via quantum emitters. Within this paradigm of a quantum network, a highly efficient and reliable interface between flying photons and stationary emitters is a prerequisite for building quantum networks [8,9].

A cavity strongly coupled to a quantum emitter is a well-known photon-emitter interface. It can accomplish a variety of elementary quantum information processing (QIP) tasks [10–12], ranging from single-photon sources [13–16] to quantum gates [17–23], quantum memories [24], and quantum routers [25–32]. However, constructing a multinode quantum network requires an array of strongly coupled cavities in a cascaded arrangement. Despite all this remarkable experimental progress, it remains a difficult technical challenge to connect different cavities while maintaining the required strong coupling [33].

Nanoscale optical waveguides provide an intriguing alternative to cavities as an efficient interface between a single photon and a single atom. In a one-dimensional (1D) nanoscale optical waveguide, photon fields are tightly confined in the transverse direction, so that a photon can interact strongly with a nearby atom [34,35]. Conversely, atoms can act as quantum scatterers for photons and control the photon propagation along the waveguide. Near-unity coupling efficiency of a quantum emitter to a photonic-crystal waveguide has been achieved experimentally [36]. Moreover, waveguides are

naturally scalable and can be easily integrated on a chip to scale up the number of nodes of a quantum network. With these attractive characteristics, coupled waveguide-emitter systems have generated tremendous interest for QIP and quantum network applications [37–47].

Recent studies of the coupled atom-waveguide system have revealed it as a versatile tool for quantum networks [37–39]. For instance, in a 1D waveguide a two-level atom strongly coupled to the optical field can be treated as a mirror with a tunable reflectivity [48–53]. A multilevel atom allows an even more flexible control of photon propagation [38,54–60]. For example, a V-type atom can act as a single-photon diode [31,61]. A  $\Lambda$ -type emitter, resonantly coupled to a single photon propagating in a 1D waveguide through one of two transitions, can flip its two ground states and simultaneously emit a photon coupled to the other transition with a probability up to 50% [62]. Even more interestingly, when the two transitions of a  $\Lambda$ -type atom are driven by the same waveguide mode [54], an effective flip of the two atomic ground states can occur. This process has been exploited to perform a controlled-phase-flip gate on two atoms [63]. By introducing a Sagnac interferometer and placing the atom at a balanced point, a single-photon interference via a  $\Lambda$ -type atom can enable a deterministic frequency conversion of single photons [64].

In this paper, we propose a photon-emitter interface by coupling a  $\Lambda$ -type quantum emitter to a 1D chiral waveguide [37–39]. The photonic spin and momentum are locked for photons propagating in a 1D chiral waveguide [40–44]. Consequently, the emitter transition between each of the ground states and the excited state selectively couples to the forward- or backward-propagating photons. A single photon propagating in such a waveguide thus has a chiral interaction with the  $\Lambda$ -type emitter, with coupling strength dependent on its traveling direction. Here we show that such a chiral photon-emitter system, which we refer to as a multifunctional quantum interface (MQI), can perform a wide variety of QIP tasks useful for a quantum network. These tasks include the

\*miran@amu.edu.pl

†keyu.xia@nju.edu.cn

‡fnori@riken.jp

SWAP gate and its square root  $\sqrt{\text{SWAP}}$  (which is an entangling gate) between the emitter and a single photon, as well as using the emitter as a quantum memory of a single photon in an arbitrary superposition state. A key advantage of this chiral system is that all these quantum processes could be realized in the exact same setup using a chiral protocol. A particular function of the MQI can be selectively enabled by applying a proper detuning between the emitter and the input photon. We show that such a selection is robust against deviations from ideal scattering conditions, such as a finite bandwidth of the photon and a finite effective interaction between the emitter and the waveguide. A specific quantum function (such as the SWAP gate) can be triggered if and only if photons are injected into the setup in a specific direction, while photons injected in the opposite direction do not cause any effect. This is significantly different from standard realizations of quantum gates, such as the protocol for a photon SWAP gate discussed in Ref. [18]. In short, such a chiral quantum system could be a truly compact, versatile, and powerful addition to the development of a complex quantum network.

The rest of the article is organized as follows: In Sec. II, we present the single-photon chiral scattering process in a coupled emitter-waveguide system. In Sec. III, we propose an MQI based on single-photon chiral scattering, which enables state swapping, entanglement generation, and quantum memory. In Sec. IV, we analyze the performance of the MQI for different QIP tasks. Finally, we conclude with a brief discussion and summary in Sec. V

## II. PHOTON SCATTERING BY A CHIRAL EMITTER-WAVEGUIDE SYSTEM

The schematic of our MQI via a chiral scattering process is depicted in Fig. 1. Specifically, we consider a single (natural or artificial) three-level  $\Lambda$ -type atom [65], e.g., nitrogen-vacancy (NV) centers in diamond, which is embedded in a photonic crystal waveguide [45,46] or a nanobeam waveguide [66]. The atomic transition  $|+\rangle \leftrightarrow |E\rangle$  ( $|-\rangle \leftrightarrow |E\rangle$ ) is optically driven by the  $\sigma^+$  ( $\sigma^-$ ) polarized photon. The chiral interaction between the atom and the waveguide originates from the combination of the following properties. Through our investigation below, we refer to the right-moving (left-moving) waveguide modes as the forward-propagating (backward-propagating) modes. The forward-propagating electromagnetic field with the wave vector  $\vec{k}$  and the backward-propagating modes with the opposite wave vector ( $-\vec{k}$ ) are related to each other via  $\vec{E}_{\vec{k}} = \vec{E}_{-\vec{k}}^*$  due to the time-reversal symmetry [37,41–44]. When placing the atom in the waveguide at a point where the local in-plane electric field is circularly polarized, the two circularly polarized dipole transitions of the atom are coupled to oppositely propagating modes. The transition, driven by a  $\sigma_+$  ( $\sigma_-$ ) polarization, can only be coupled to the forward-propagating (backward-propagating)  $k$ -mode with the coupling constant  $\Gamma_f(k) = V_f^2(k)$  [ $\Gamma_b(k) = V_b^2(k)$ ].

The Hamiltonian  $\hat{H}$  is, thus, given by

$$\hat{H} = \hat{H}_0 + \hat{H}_1, \quad (1)$$

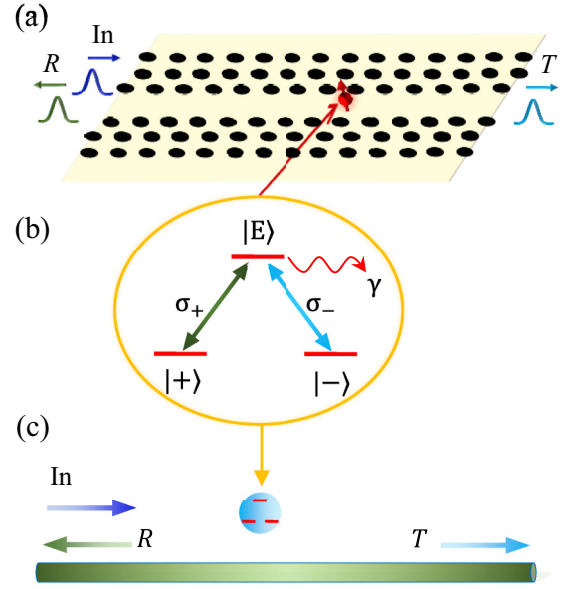


FIG. 1. (a) Chiral scattering of a single photon by a  $\Lambda$ -type emitter coupled to a photonic-crystal waveguide, (b) energy levels and the circularly polarized ( $\sigma_{\pm}$ ) dipole transitions of a  $\Lambda$ -type emitter (decaying with a damping rate  $\gamma$ ), and (c) chiral scattering of a single photon by a  $\Lambda$ -type emitter coupled to the waveguide. Here  $R$  and  $T$  represent the reflection and transmission amplitudes of the scattered output modes. For simplicity, we show only a photon entering the waveguide from its left-hand side (say, a forward-propagating photon), although we also consider a backward-propagating photon. The atom is placed at a point of the local in-plane (circular) polarization of the electric field in the waveguide (see Ref. [37] for a pedagogical description of this configuration). The circularly-polarized  $\sigma_+$  ( $\sigma_-$ ) dipole transition couples *only* to the forward- or backward-propagating modes with the coupling constants  $\Gamma_f(k) = V_f^2(k)$  or  $\Gamma_b(k) = V_b^2(k)$ , respectively.

where the free Hamiltonian  $\hat{H}_0$  and the interaction Hamiltonian  $\hat{H}_1$  can be given in the dipole and rotating-wave approximation, respectively, as

$$\begin{aligned} \hat{H}_0 &= \Omega_E \hat{\sigma}_{EE} + \sum_{j=\pm} \left[ \int_0^{\infty} dk \omega_{jf}(k) \hat{a}_{jf}^{\dagger}(k) \hat{a}_{jf}(k) \right. \\ &\quad \left. + \int_{-\infty}^0 dk \omega_{jb}(k) \hat{a}_{jb}^{\dagger}(k) \hat{a}_{jb}(k) \right], \quad (2) \\ \hat{H}_1 &= \int dk [V_f(k) \hat{a}_{+f}^{\dagger}(k) \hat{\sigma}_{+E} + V_b(k) \hat{a}_{-b}^{\dagger}(k) \hat{\sigma}_{-E} + \text{H.c.}], \quad (3) \end{aligned}$$

where, for simplicity, we set the group velocity  $c = 1$  and  $\hbar = 1$ , the frequency of a single photon is assumed to be identical to its absolute value of the wave vector ( $\omega_k = |k|$ ), and the energy of the atomic ground states  $|\pm\rangle$  is assumed to be zero. Moreover,  $\hat{\sigma}_{iE} = |i\rangle\langle E|$  with  $i = \pm$ ,  $E$  are the atomic transition operators, and  $\Omega_E$  is the optical-transition frequency of the atom. This chiral Hamiltonian, given in Eq. (1), is a generalization of standard Hamiltonians describing a nonchiral interaction of a multimode electromagnetic field and a two-level [67] or three-level [62] atom. The creation operator  $\hat{a}_{jf}^{\dagger}(\omega)$  [ $\hat{a}_{jb}^{\dagger}(\omega)$ ] creates a  $j$ -polarized photon of fre-

quency  $\omega$  in the forward-propagating (backward-propagating) modes along the waveguide. As considered in previous works [34–39], a linearized dispersion relation of photons around the frequency  $\omega_0 = |\pm \vec{k}_0|$  of an input photon is used here with  $\omega_{jf}(\vec{k}) = \omega_0 + k - k_0$  and  $\omega_{jb}(-\vec{k}) = \omega_0 - k + k_0$ . In addition, all the couplings are taken to be constant  $V_f(k) = V_b(k) = V/\sqrt{2}$ , because  $|V_f(k)|^2$  and  $|V_b(k)|^2$  are much less than  $\omega_0$  and vary slowly around  $k_0$ . This is a direct result of the memoryless character of the photonic field, known as the Markov approximation [67,68].

In the quantum-jump (or quantum-trajectory) approach, the dissipative time evolution is described by a non-Hermitian effective Hamiltonian [67,68]:

$$\hat{H}_{\text{eff}} = \hat{H} - i\frac{\gamma}{2}\hat{\sigma}_{EE}, \quad (4)$$

where the imaginary term  $i\gamma/2$ , with the damping constant  $\gamma$ , refers in our model to a nondirectional spontaneous emission of the excited state  $|E\rangle$ . The evolution, governed by Hamiltonian (4), can be interrupted by random quantum jumps. However, we study the conditional dynamics, which is described only by the non-Hermitian Hamiltonian  $\hat{H}_{\text{eff}}$  without quantum jumps, since the dissipation results in detectable photon loss [67].

After transforming the Hamiltonian (4) into the frame rotating with input-photon frequency  $\omega_0$ , the integration ranges in Eqs. (2) and (3) can be extended to  $(-\infty, \infty)$  for performing the Fourier transform of the field operators, because only a narrow bandwidth in the vicinity of  $\omega_0$  will be taken into consideration and has a nontrivial contribution to the final scattering process. The dynamics of the system consisting of a  $\Lambda$ -type atom and a waveguide is described by the Hamiltonian  $\tilde{H}_{\text{eff}}$  in real space as follows:

$$\begin{aligned} \tilde{H}_{\text{eff}} &= \tilde{H}_0 + \tilde{H}_1, \\ \tilde{H}_0 &= \tilde{\Delta}\hat{\sigma}_{EE} - i \int dx [\hat{a}_f^\dagger(x)\partial_x\hat{a}_f(x) - \hat{a}_b^\dagger(x)\partial_x\hat{a}_b(x)], \\ \tilde{H}_1 &= \int dx \delta(x) [\sqrt{\Gamma_f}\hat{a}_f^\dagger(x)\hat{\sigma}_{+E} + \sqrt{\Gamma_b}\hat{a}_b^\dagger(x)\hat{\sigma}_{-E} + \text{H.c.}]. \end{aligned} \quad (5)$$

Here  $\delta(x)$  is the Dirac  $\delta$  function modeling the scattering point at  $x = 0$ , where the atom is placed. The effective detuning between the atom and an input photon is

$$\tilde{\Delta} = \omega_A - \Omega_E + i\gamma/2.$$

Moreover,  $\hat{a}_{f,b}(x)$  [ $\hat{a}_{f,b}^\dagger(x)$ ] annihilates (creates) a forward-propagating (backward-propagating) propagating photon at the point  $x$ . These operators are related to the corresponding operators in the wave-vector representation by the Fourier transforms:

$$\begin{aligned} \hat{a}_f(x) &= \frac{1}{2\pi} \int dk \hat{a}_f(k) e^{ikx}, \\ \hat{a}_b(x) &= \frac{1}{2\pi} \int dk \hat{a}_b(k) e^{-ikx}. \end{aligned} \quad (6)$$

To study the scattering of a single photon with frequency  $\omega_A$  by this atom-waveguide system, one should consider two cases: (1) If a given input photon does *not* match a circularly polarized transition of the atom, then it propagates in the forward modes

in the waveguide without any disturbance; however, (2) if an input photon matches a given transition, then it strongly couples to the atom. Note that forward-propagating (backward-propagating) modes evolve into the circularly polarized state  $|\sigma_+\rangle$  ( $|\sigma_-\rangle$ ) at the position of the atom. Thus, if the atom is initially prepared in the state  $|+\rangle$ , the quantum state of a forward-propagating photon changes significantly due to scattering from the atom. Otherwise, it passes through the atom without change.

For calculating the reflection and transmission amplitudes, we first give a general state of the single-excitation subspace of the system composed of the atom and waveguide modes [35], which reads as

$$\begin{aligned} |\psi_1\rangle &= \phi_E |\Phi, E\rangle + \int dx \phi_f(x) \hat{a}_f^\dagger(x) |\Phi, +\rangle \\ &+ \int dx \phi_b(x) \hat{a}_b^\dagger(x) |\Phi, -\rangle, \end{aligned} \quad (7)$$

where  $\hat{a}_f^\dagger(x) |\Phi\rangle$  [ $\hat{a}_b^\dagger(x) |\Phi\rangle$ ] denotes a forward-propagating (backward-propagating) photon at the point  $x$  with single-photon wave function  $\phi_f(x)$  [ $\phi_b(x)$ ],  $|\Phi\rangle$  denotes the vacuum state for optical-field operators, and  $\phi_E$  represents the probability amplitude that the atom is excited to the state  $|E\rangle$ . We can then give a set of equations resulting from the time-independent Schrödinger equation  $\tilde{H}_{\text{eff}} |\psi_1\rangle = \omega_A |\psi_1\rangle$ :

$$\begin{aligned} 0 &= (-i\partial_x - \omega_A)\phi_f(x) + \sqrt{\Gamma_f}\delta(x)\phi_E, \\ 0 &= (i\partial_x - \omega_A)\phi_b(x) + \sqrt{\Gamma_b}\delta(x)\phi_E, \\ 0 &= -\tilde{\Delta}\phi_E + \sqrt{\Gamma_f}\phi_f(0) + \sqrt{\Gamma_b}\phi_b(0). \end{aligned} \quad (8)$$

We assume the following ansatz for the solutions of the above equations:

$$\begin{aligned} \phi_f(x) &= \exp(ik_f x) [\Theta_H(-x) + T\Theta_H(x)], \\ \phi_b(x) &= \exp(-ik_b x) R\Theta_H(-x), \end{aligned} \quad (9)$$

where  $T$  and  $R$  are the transmission and reflection probability amplitudes of this atom-waveguide system, and  $\Theta_H(x)$  is the Heaviside step function with  $\Theta_H(x)|_{x=0} = 1/2$  and  $\frac{\partial\Theta_H(x)}{\partial x}|_{x=0^+} = 1$ . The set of equations, given in Eq. (8), evolves into

$$\begin{aligned} 0 &= (k_f - \omega_A)\phi_f(x) - ie^{ik_f x}\delta(x)[T - 1] + \sqrt{\Gamma_f}\delta(x)\phi_E, \\ 0 &= (k_b - \omega_A)\phi_b(x) - ie^{-ik_b x}\delta(x)R + \sqrt{\Gamma_b}\delta(x)\phi_E, \\ 0 &= -\tilde{\Delta}\phi_E + \sqrt{\Gamma_f}\phi_f(0) + \sqrt{\Gamma_b}\phi_b(0). \end{aligned} \quad (10)$$

After inserting the solution ansatz into the above equations, we directly obtain

$$\begin{aligned} \phi_E &= \frac{2\sqrt{\Gamma_f}}{2\tilde{\Delta} + i(\sqrt{\Gamma_b}\Gamma_f + \Gamma_b)}, \\ R &= -i\sqrt{\Gamma_b}\phi_E, \\ T &= \frac{2\tilde{\Delta} + i(\Gamma_b - \sqrt{\Gamma_b}\Gamma_f)}{2\sqrt{\Gamma_f}}\phi_E, \end{aligned} \quad (11)$$

It could easily be found that an input photon in a proper direction is totally reflected with  $R = -1$  and  $T = 0$  in the ideal resonant scattering process, assuming no detuning,  $\Delta =$

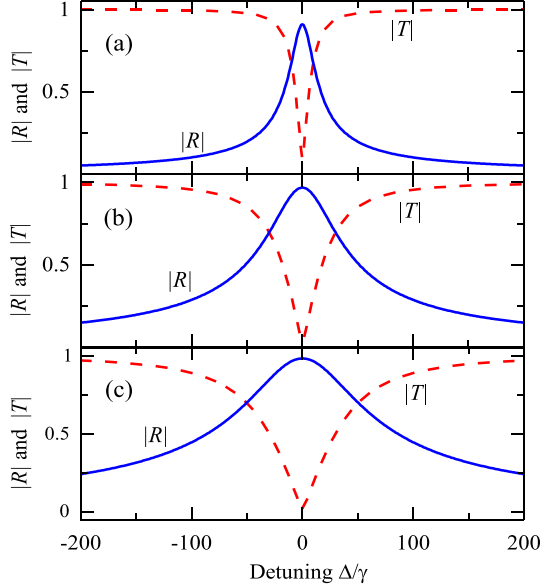


FIG. 2. Absolute values of the transmission  $|T|$  and reflection  $|R|$  amplitudes versus the detuning  $\Delta$  (in units of the damping rate  $\gamma$ ) between an input photon and the atomic transitions with (a)  $\beta = 10$ , (b)  $\beta = 30$ , and (c)  $\beta = 50$ . Here  $\beta = \Gamma/\gamma$  is the ratio of the coupling constant  $\Gamma$  and the damping rate  $\gamma$  describing the enhancement of the directional emission of the atom.

$\omega_A - \Omega_E = 0$ , and the same coupling rates  $\Gamma_b = \Gamma_f = \Gamma$ , which are much greater than the damping rate, i.e.,  $\Gamma \gg \gamma$ . This means that we assume the strong-coupling regime [34]. At the same time, the ground state of the atom is flipped into the other one. That is, a perfect single-photon scattering process is completed and the photon state and the ground states of the  $\Lambda$ -type atom are flipped simultaneously.

Before analyzing a possible application of the MQI for QIP, we first study the transmission and reflection amplitudes versus practical parameters: the photon detuning  $\Delta$  and the ratio  $\beta = \Gamma/\gamma$  of the coupling and damping rates showing the enhancement of the directional emission of the atom, shown in Fig. 2. The absolute values of the transmission and reflection amplitudes,  $|T|$  and  $|R|$ , in Eq. (11) are obtained from the stationary solutions in real space. Furthermore, we numerically verify these amplitudes  $T$  and  $R$  by solving the time-dependent Schrödinger equation  $-i \frac{\partial |\psi\rangle}{\partial t} = \hat{H}_{\text{eff}} |\psi\rangle$ , where  $|\psi\rangle$  denotes a general single-excitation state in the wave-vector space and evolves under the wave-vector space Hamiltonian  $\hat{H}_{\text{eff}}$  in Eq. (4), and the wave-vector distribution of an input photon is assumed to be a Gaussian pulse,

$$f(k) = \frac{5}{k_0 \sqrt{\pi}} \exp[-(k - k_0)^2 (5/k_0)^2]. \quad (12)$$

On the scale of Fig. 2, there is no difference between the analytical results and the corresponding numerical calculations.

It is clearly seen that there are three distinct detuning points for a single-photon scattering process, involving the atom-waveguide discussed here. One of those is the resonant point, where the input single photon is almost deterministically reflected with the atomic ground state flipped, and the largest difference is observed between the reflection and transmission

modes. While at the other two points for the detuning  $\Delta \approx \pm\Gamma$ , the scattered photon propagates with equal probability in the reflection and transmission modes and the atom is projected into the corresponding ground state, which leads to an entanglement between the ground states of the  $\Lambda$ -type atom and the photon state [69].

### III. MULTIFUNCTIONAL QUANTUM INTERFACE FOR QIP

The proposed system, consisting of a  $\Lambda$ -type atom and a nanowaveguide, provides a deterministic quantum interface between a single photon and a single atom. When a photon is injected in the direction that excites a local circularly polarized field that the atom is coupled to, then the photon is either reflected along with a ground-state flip of the atom or keeps propagating in the transmission modes, leaving the atom without changing its original state. The relative probabilities of these two scattering modes can be controlled by the detuning  $\Delta$ . In this section, we describe a MQI as an elementary building block of chiral quantum networks. The SWAP gate, the quantum memory, and a hybrid-entangling gate between a single atom and a polarized-encoded single photon could, in principle, be implemented in the same setup that is triggered only when a polarized-encoded photon is input in a particular port. When a photon enters the MQI from the other port, it passes through the setup with a polarization flip, leaving the atom unchanged. This provides potential applications for chiral quantum networks when multiple channels, linking different nodes, are tunable [39].

#### A. General scattering output matrix

The setup for chiral QIP with polarized-encoded single photons is shown in Fig. 3(a). It is composed of a dominant nanowaveguide coupled to a  $\Lambda$ -type atom and several linear optical elements: a polarized beam splitter (PBS), an optical circulator (OC), and a polarization controller (PC). The PBS transmits horizontally polarized photons (state  $|H\rangle$ ) and reflects vertically polarized photons (state  $|V\rangle$ ). The PC flips the polarization of a photon passing through it and performs the conversion  $|H\rangle \leftrightarrow |V\rangle$ , while the OC is used to spatially separate the input and output modes [17–19] by transmitting an input photon in one port to an output port determined by the operation direction of the circulator.

A single photon encoded in the superposition polarization state  $|\psi_p\rangle = \alpha_H |H\rangle + \alpha_V |V\rangle$  is split into two directions by the PBS, followed by a polarization flip on the transmission modes. Therefore, a single photon passing through either the right or left OC has the same polarization, which maximally couples the photon into a waveguide from either direction and creates a right- ( $|\sigma_+\rangle$ ) or left- ( $|\sigma_-\rangle$ ) circularly polarized local field at the atom position [37–44,66]. For the atom initialized in the state  $|\psi_A\rangle = \beta_+ |+\rangle + \beta_- |-\rangle$ , the combined atom-photon state evolves into

$$\begin{aligned} |\psi_1\rangle = & \beta_+ (T\alpha_V |\sigma_+, +\rangle + R\alpha_V |\sigma_-, -\rangle) \\ & + \beta_- (T\alpha_H |\sigma_-, -\rangle + R\alpha_H |\sigma_+, +\rangle) \\ & + \beta_+ \alpha_H |\sigma_-, +\rangle + \beta_- \alpha_V |\sigma_+, -\rangle. \end{aligned} \quad (13)$$

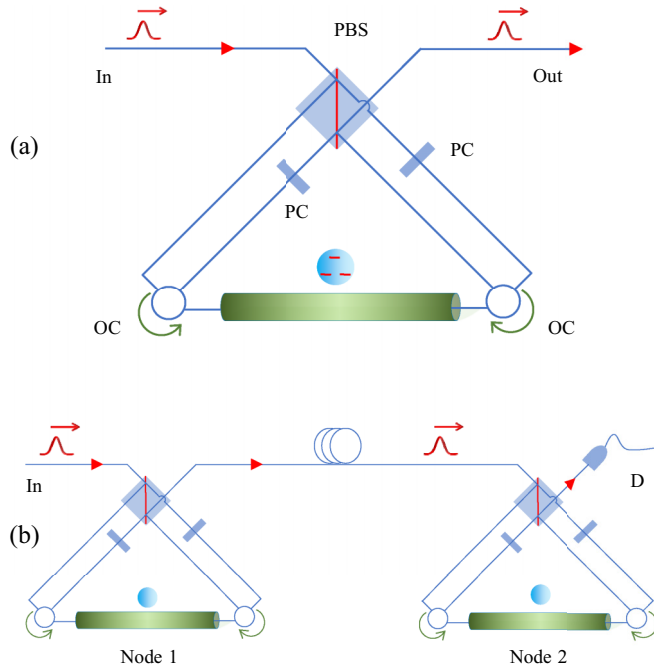


FIG. 3. (a) Schematics of the multifunctional quantum interface (MQI) using a  $\Lambda$ -type emitter and a 1D waveguide and (b) heralded-entanglement generation and quantum-state transmission between two remote quantum nodes. Here, PBS denotes a polarized beam splitter, OC is an optical circular, and PC is a polarization controller.

According to the time-reversal symmetry of the waveguide, the polarization of a photon evolves into the vertically polarized state  $|V\rangle$ , and it is rerouted by the OCs followed by a polarization flip on the left-propagating modes. Subsequently, the two propagating modes of the photon recombine together at the PBS, and the combined system evolves into the state  $|\psi_2\rangle$ , when the photon is leaving the PBS:

$$\begin{aligned}
 |\psi_2\rangle = & \beta_+ |H\rangle (R\alpha_v |-\rangle + \alpha_H |+\rangle) \\
 & + \beta_- |V\rangle (\alpha_v |-\rangle + R\alpha_H |+\rangle) \\
 & + T(\beta_+ \alpha_v |V, +\rangle + \beta_- \alpha_H |H, -\rangle). \quad (14)
 \end{aligned}$$

This process could be described by a general scattering matrix  $\hat{S}$  that connects the initial and final states of the combined system consisting of a polarized photon and a  $\Lambda$ -type atom as

$$|\psi_2\rangle = \hat{S} |\psi_A\rangle |\psi_P\rangle, \quad (15)$$

where

$$\hat{S} = \begin{pmatrix} 1 & 0 & 0 & 0 \\ 0 & T & R & 0 \\ 0 & R & T & 0 \\ 0 & 0 & 0 & 1 \end{pmatrix}. \quad (16)$$

### B. Quantum gates and memory

In general, specific functions of the MQI depend on the reflection and transmission amplitudes,  $R$  and  $T$ , which are tunable by controlling the detuning between an input photon and the atom. By properly selecting scattering conditions, the

atom-waveguide system evolves as intended, leading to desired functions of the MQI.

#### 1. SWAP gate

As discussed in the previous section, when the frequency of an input photon is nearly resonant with the atom, the photon is deterministically reflected by the atom. Simultaneously, the state of the atom is flipped, with  $R = -1$  and  $T = 0$  for an ideal directional scattering process, if the coupling constant is much greater than the damping rate, i.e.,  $\Gamma \gg \gamma$ , which corresponds to the strong-coupling regime. Therefore, the general scattering matrix  $\hat{S}$  is simplified to

$$\hat{S}_{\Delta=0} = \begin{pmatrix} 1 & 0 & 0 & 0 \\ 0 & 0 & -1 & 0 \\ 0 & -1 & 0 & 0 \\ 0 & 0 & 0 & 1 \end{pmatrix}. \quad (17)$$

Obviously, this scattering process equivalently performs the standard SWAP gate between a polarized photon and a single atom, because the  $\pi$ -phase shift could be completely compensated by local phase-flip operations  $\hat{\sigma}_z$ :

$$\text{SWAP} = (\hat{I} \otimes \hat{\sigma}_z) \hat{S}_{\Delta=0} (\hat{I} \otimes \hat{\sigma}_z), \quad (18)$$

where  $\hat{I}$  is the qubit identity operator.

#### 2. Quantum memory

In order to perform the quantum memory of a single photon encoded in an arbitrary polarization state, one can first perform the SWAP gate, as described above, and then perform a measurement of the scattered photon to guarantee that the SWAP gate has been completed and the state of the polarized photon is now stored in the atom. After a while, to read out the state of the original photon, one can perform another SWAP gate by impinging another photon. Although the second photon could, in principle, be initially in an arbitrary pure state or even a mixed state, here, for simplicity, we assume that the initial polarized photon state is  $|V\rangle$ . The atom, in an ideal scattering process, is mapped into the ground state  $|-\rangle$  and a photon of the same polarization as that of the original photon is generated simultaneously. Thus, these operations store and retrieve a single-photon state, which completes the quantum memory procedure.

#### 3. $\sqrt{\text{SWAP}}$ gate

The setup shown in Fig. 3(a) could also be exploited to generate entanglement between a polarized photon and a single atom, which can be referred to as hybrid entanglement. Instead of working near the resonant point, one introduces a detuning of  $(\pm\Gamma)$  for a given input photon. Now the general scattering matrix, shown in Eq. (16), is specified as follows:

$$\hat{S}_{\Delta=\Gamma} = \begin{pmatrix} 1 & 0 & 0 & 0 \\ 0 & -\frac{i-1}{2} & -\frac{1+i}{2} & 0 \\ 0 & -\frac{1+i}{2} & -\frac{i-1}{2} & 0 \\ 0 & 0 & 0 & 1 \end{pmatrix} \quad (19)$$

and

$$\hat{S}_{\Delta=-\Gamma} = \hat{S}_{\Delta=\Gamma}^{-1} = \begin{pmatrix} 1 & 0 & 0 & 0 \\ 0 & \frac{1+i}{2} & -\frac{1-i}{2} & 0 \\ 0 & -\frac{1-i}{2} & \frac{1+i}{2} & 0 \\ 0 & 0 & 0 & 1 \end{pmatrix}. \quad (20)$$

By applying  $\hat{S}_{\Delta=\Gamma}$  or  $\hat{S}_{\Delta=-\Gamma}$  on a hybrid system consisting of a single atom and a polarized photon,  $|\psi_A\rangle|\psi_P\rangle$ , the square root of the SWAP gate ( $\sqrt{\text{SWAP}}$ ) is accomplished in this system, because

$$(\hat{S}_{\Delta=\Gamma})^2 = (\hat{S}_{\Delta=-\Gamma})^2 = \hat{S}_{\Delta=0}. \quad (21)$$

We note that our gate, given in Eq. (20), differs from the standard  $\sqrt{\text{swap}}$  gate only by local operations, i.e.,

$$\sqrt{\text{SWAP}} = (\hat{I} \otimes \hat{\sigma}_z) \hat{S}_{\Delta=-\Gamma} (\hat{I} \otimes \hat{\sigma}_z). \quad (22)$$

Thus, our system can be used to generate the maximal entanglement between a polarized photon and a single atom, by initializing these to be in the state  $|H\rangle|+\rangle$  or  $|V\rangle|-\rangle$ . When combined with the classical swapping procedure described above, one can establish the maximal entanglement between two remote atoms placed at different nodes of quantum networks, as shown in Fig. 3(b).

So far, we have described the SWAP gate, the quantum memory, and the hybrid-entangling  $\sqrt{\text{SWAP}}$  gate, based on the effective scattering of the atom-waveguide system. However, if one switches the output port of the MQI to be a new input port, one can easily find that the probability amplitude of the input polarized photon is first divided into two amplitudes of propagating modes, and then the photon exhibits a polarization flip. These modes are directly transmitted to the PBS by any of the OCs. Finally, the photon reaches the PBS with a polarization flip from the original input port of the MQI. In summary, when a photon enters at a particular input port, it enables the MQI to perform various QIP tasks, while the photon enters from the other input port then just passes through the MQI leaving the atom unaffected. This provides an interesting application for complex quantum networks when multiple connecting channels are available, because the quantum function of the MQI could be switched on or off for various QIP tasks simply by choosing different connecting channels.

#### IV. FIDELITY AND EFFICIENCY OF QIP WITH MQI

In the previous section, we described the MQI for unidirectional implementations of the SWAP and  $\sqrt{\text{SWAP}}$  gates, and quantum memory, for all the tasks which, in principle, work in a deterministic way. However, the practical scattering output of the MQI can deviate from the ideal outcome due to the finite linewidth of the input photon and the nondirectional spontaneous emission of the atom. Here we use both the average fidelity  $\bar{F}$  and the average efficiency  $\bar{\eta}$  to evaluate the performance of the MQI for different QIP tasks.

For the SWAP and quantum hybrid-entangling  $\sqrt{\text{SWAP}}$  gates, the fidelities and efficiencies depend on the states of the atom and the photon involved. To evaluate the performance of these processes, one can use the average fidelity and efficiency [5,70,71]. The average fidelity  $\bar{F}$  is defined as the average overlap between the ideal and the practical outputs for different

photonic and atomic states. Thus, the average fidelities for the SWAP and  $\sqrt{\text{SWAP}}$  gates read, respectively, as

$$\bar{F}_{\text{swap}} = \frac{1}{N} \sum_{i=1}^N \sqrt{\frac{|\langle \psi_i | \hat{S}_{\Delta=0}^\dagger | \psi_{\text{swap}}^{(i)} \rangle|^2}{\langle \psi_{\text{swap}}^{(i)} | \psi_{\text{swap}}^{(i)} \rangle}}, \quad (23)$$

$$\bar{F}_{\text{ent}} = \frac{1}{N} \sum_{i=1}^N \sqrt{\frac{|\langle \psi_i | \hat{S}_{\Delta=\Gamma}^\dagger | \psi_{\text{ent}}^{(i)} \rangle|^2}{\langle \psi_{\text{ent}}^{(i)} | \psi_{\text{ent}}^{(i)} \rangle}}, \quad (24)$$

where  $\hat{S}_{\Delta=0}$  and  $\hat{S}_{\Delta=\Gamma}$  are the ideal transition matrices given, respectively, in Eqs. (17) and (19), and  $|\psi_{\text{swap}}^{(i)}\rangle$  ( $|\psi_{\text{ent}}^{(i)}\rangle$ ) is the corresponding output state obtained from the frequency-dependent scattering matrix resulting from Eq. (16). Moreover,  $|\psi_i\rangle$  is a state chosen from the overcomplete set of  $N = 36$  states:  $\{|+\rangle, |-\rangle, (|+\rangle \pm |-\rangle)/\sqrt{2}, (|+\rangle \pm i|-\rangle)/\sqrt{2}\} \otimes \{|H\rangle, |V\rangle, (|H\rangle \pm |V\rangle)/\sqrt{2}, (|H\rangle \pm i|V\rangle)/\sqrt{2}\}$ , where

$$|j\rangle = \int d\omega f(\omega) \hat{a}_j^\dagger(\omega) |\Phi\rangle, \quad (25)$$

where ( $j = H, V$ ) represents a single-photon pulse of the frequency distribution  $f(\omega)$ .

When the MQI is used to perform the quantum memory for an arbitrary single-photon pulse, an initially separable state of the combined system, consisting of a single photon and an atom, is modified due to its nonzero transmission in a practical scattering process. In order to increase the fidelity of the quantum memory, one can initially prepare the atom in a deterministic state  $|-\rangle$ . After the storage and read-out processes, the measurement on the atom in the basis  $\{|+\rangle, |-\rangle\}$  is performed. The average fidelity conditioned on the measurement of the atom to the state  $|-\rangle$  is given by

$$\bar{F}_{\text{mem}} = \frac{1}{N} \sum_{i=1}^N \sqrt{\frac{|\langle \phi_i | \psi_{\text{mem}}^{(i)} \rangle|^2}{\langle \psi_{\text{mem}}^{(i)} | \psi_{\text{mem}}^{(i)} \rangle}}, \quad (26)$$

where  $N = 6$ ;  $|\phi_i\rangle$  is chosen from the overcomplete set of states  $\{|H\rangle, |V\rangle, (|H\rangle \pm |V\rangle)/\sqrt{2}, (|H\rangle \pm i|V\rangle)/\sqrt{2}\}$ ; and  $|\psi_{\text{mem}}^{(i)}\rangle = \hat{M}|\phi_i\rangle$  is the realistic output state with the following frequency-dependent filter matrix:  $\hat{M} = \begin{pmatrix} R^2 & 0 \\ T & 1 \end{pmatrix}$ .

Moreover, the average efficiencies  $\bar{\eta}_k$  can be given by the average probabilities of observing directional scattering, i.e.,

$$\bar{\eta}_k = \frac{1}{N} \sum_{i=1}^N \langle \psi_k^{(i)} | \psi_k^{(i)} \rangle. \quad (27)$$

In special cases, this formula reduces to  $\bar{\eta}_{\text{swap}}$ ,  $\bar{\eta}_{\text{ent}}$ , and  $\bar{\eta}_{\text{mem}}$ , which are shown in Figs. 4 and 5.

The performance of the quantum gates and memory via the MQI are shown in Fig. 4, where we plotted the fidelities and the efficiencies versus the effective directional scattering rate  $\Gamma/\gamma$  for a given Gaussian single-photon pulse defined by the spectrum

$$f(\omega) = \frac{1}{\sqrt{\pi}\sigma_\omega} \exp\left[-\left(\frac{\omega - \omega_c}{\sigma_\omega}\right)^2\right], \quad (28)$$

where  $\omega_c$  is the center frequency and  $\sigma_\omega$  denotes the pulse bandwidth. In general, the MQI implements the SWAP and  $\sqrt{\text{SWAP}}$  gates better than the quantum memory. This is because only

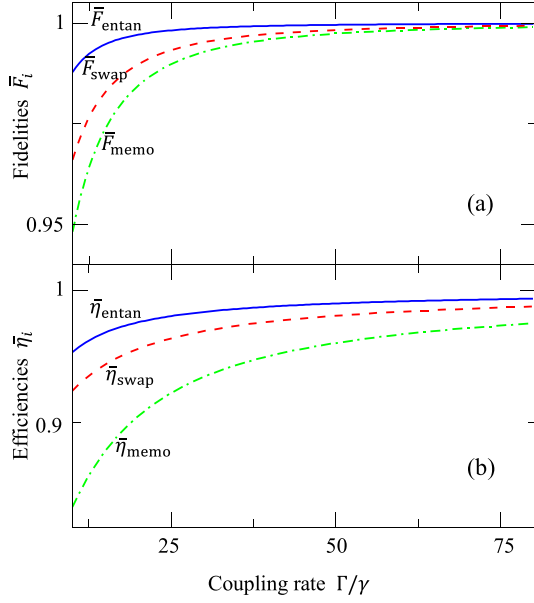


FIG. 4. (a) The average fidelities  $\bar{F}_{\text{ent}}$ ,  $\bar{F}_{\text{swap}}$ , and  $\bar{F}_{\text{mem}}$  and (b) the average efficiencies  $\bar{\eta}_{\text{ent}}$ ,  $\bar{\eta}_{\text{swap}}$ , and  $\bar{\eta}_{\text{mem}}$  versus the coupling constant  $\Gamma$  (in units of the damping rate  $\gamma$ ). The averages are calculated over all detunings of an input photon, with the Gaussian wave form given by Eq. (28) with  $\sigma_{\omega} = 5\gamma$ .

one nonideal single-photon scattering process is involved in our implementation of the gates, while two scattering processes are involved for realizing a quantum memory. For the  $\sqrt{\text{SWAP}}$  gate, both the average fidelity and the average efficiency approach their respective stable values of  $\bar{F}_{\text{ent}} = 0.9996$  and

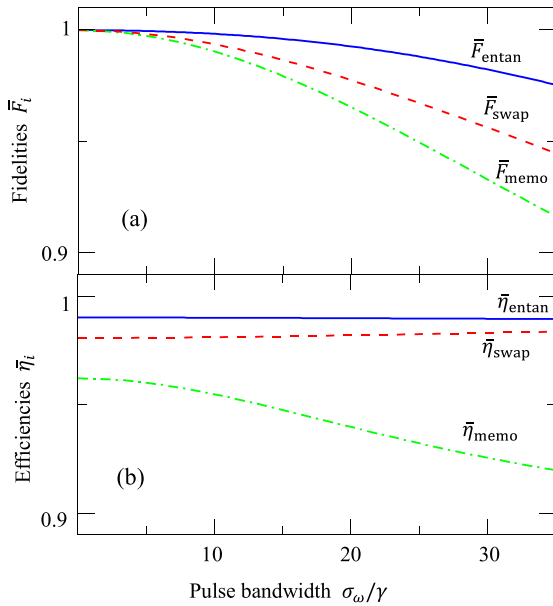


FIG. 5. (a) Average fidelities  $\bar{F}_{\text{ent}}$ ,  $\bar{F}_{\text{swap}}$ , and  $\bar{F}_{\text{mem}}$  and (b) average efficiencies  $\bar{\eta}_{\text{ent}}$ ,  $\bar{\eta}_{\text{swap}}$ , and  $\bar{\eta}_{\text{mem}}$  versus the pulse bandwidth  $\sigma_{\omega}/\gamma$  (in units of the damping rate  $\gamma$ ). These averages are calculated over all detunings of an input photon, with the Gaussian wave form given by Eq. (28) and  $\Gamma/\gamma = 50$ .

$\bar{\eta}_{\text{ent}} = 0.9901$  when the directional scattering rate is  $\Gamma/\gamma \geq 50$  for a narrow input-photon pulse  $\sigma_{\omega} = 5\gamma$ . For the SWAP gate, the average fidelity and efficiency are almost as high as those for the  $\sqrt{\text{SWAP}}$  gate, with  $\bar{F}_{\text{swap}} = 0.9982$  and  $\bar{\eta}_{\text{swap}} = 0.9810$ , for  $\Gamma/\gamma \geq 50$ . The fidelity and efficiency of the quantum memory are slightly lower than those for the two gates. The average fidelity and average efficiency of the quantum memory are still large enough for a practical quantum network, because  $\bar{F}_{\text{mem}} \geq 0.9928$  and  $\bar{\eta}_{\text{mem}} \geq 0.9345$  are achievable for the effective directional scattering rate  $\Gamma/\gamma \geq 30$ .

To study the influence of the bandwidth of an input photon, the performances of all three functions of the MQI are shown in Fig. 5 for the ratio of the directional coupling constant and damping rate,  $\Gamma/\gamma = 50$ . In general, the average fidelities of all three functions decrease with increasing the bandwidth  $\sigma_{\omega}/\gamma$  of the single-photon pulse. This is because the increment of  $\Gamma/\gamma$  leads to a larger deviation from the ideal scattering condition for each quantum process. However, this larger deviation compensates partially other detrimental effects and contributes to the average efficiency of the SWAP and  $\sqrt{\text{SWAP}}$  gates, because the wide bandwidth leads to a larger detuning at the edge range that contributes less to a realistic scattering, resulting in a smaller absorption for the subsequent nondirectional emission. Furthermore, the MQI performs excellently for the three QIP tasks when  $\sigma_{\omega}/\gamma \leq 25$ . The lowest performance among these three tasks is for the quantum memory, which has an average fidelity of  $\bar{F}_{\text{mem}} \geq 0.95$  and an average efficiency of  $\bar{\eta}_{\text{mem}} \geq 0.92$ .

So far we have assumed that the optical circulator (OC) has perfect efficiency. Nevertheless, realistic OCs always cause some small losses of photons passing through them [72]. For example, a waveguide-based OC with a loss rate of 0.05 dB has been designed and simulated [73]. Moreover, photon losses introduced by OCs only slightly reduce the fidelity of an MQI, because an OC reduces equally both polarization components of a single photon. In this respect, an OC can be replaced by an unbalanced beam splitter [22,23].

To date, single-photon sources of narrow bandwidth based on both natural and artificial atoms have been significantly improved [13–15,74]. Nevertheless, solid-state single-photon sources still suffer from spectral diffusion and dephasing caused by phonons. These effects limit the application of such photons for practical QIP tasks [74]. Fortunately, such spectral broadening can be partially suppressed at low temperatures and by coupling emitters to optical cavities or waveguides. For example, a Fourier-transform-limited source based on NV centers in nanocrystals has been demonstrated with a linewidth of 16 MHz at cryogenic temperatures [75]. Narrowband single photons could also be efficiently generated by a three-level emitter, strongly coupled to a high-finesse optical cavity, with vacuum-stimulated Raman transitions [13–15]. Furthermore, a solid-state single-photon source of subnatural linewidth has been demonstrated by operating in the small Rabi frequency limit of resonance fluorescence [76].

The dominant element of the MQI is the chiral interaction between a  $\Lambda$ -type atom and a single photon in a waveguide. A promising implementation is a single negatively charged NV center coupled to a photonic-crystal waveguide. Here the states  $|\pm\rangle$  of the  $\Lambda$ -level structure, shown in Fig. 1(b), are the ground states of the NV center with magnetic numbers  $m_s =$

$\pm 1$  associated with the orbital angular momentum  $m_l = 0$ . The excited state  $|E\rangle$  is given by the state

$$|A_2\rangle = \frac{1}{\sqrt{2}}(|+1\rangle|E_-\rangle + |-1\rangle|E_+\rangle)$$

of the NV center, where  $|E_{\pm}\rangle$  are the orbital states with angular momentum  $m_l = \pm 1$ , and  $|\pm 1\rangle$  are the spin states with magnetic numbers  $m_s = \pm 1$  [69,77–79]. According to the total angular momentum conservation, the transition  $|+\rangle \leftrightarrow |E\rangle$  ( $|-\rangle \leftrightarrow |E\rangle$ ) is accompanied by the absorption or radiation of a single  $\sigma_+$  ( $\sigma_-$ ) polarized photon, and it has been used to generate quantum entanglement involving polarized photons [69,77].

A photonic-crystal waveguide is a well-developed one-dimensional system for enhancing the effective interaction between a flying photon and a solid-state emitter [10]. A strong coupling between an emitter and a waveguide with  $\Gamma/\gamma \simeq 50$  has been demonstrated [36]. A waveguide photon can also be collected by a grating, a tapered-mode adapter, or even a fiber for subsequent operations [36,80–82]. By using glide-plane waveguides, the maximum interaction between an atom and a waveguide is achieved for unidirectional scattering, because a chiral point corresponds to the field maximum of the waveguide [82,83]. Moreover, regular nanobeam waveguides and nanofibers coupled to NV center or other three-level  $\Lambda$ -type emitters could also be used to build this MQI [84–86].

## V. DISCUSSION AND SUMMARY

The chiral interaction between a single photon in a waveguide and a quantum emitter has gained considerable attention [37–39,45,46]. It combines the advantages of both a chiral waveguide system and a controllable  $\Lambda$ -type emitter system. The spin-momentum-locked light in the chiral waveguide changes its polarization when its direction is reversed [41–44]. This leads to a totally different scattering when it is coupled to single emitters with polarization-dependent dipole transitions. That is, either zero- or  $\pi$ -phase shift occurs on the transmitted modes conditioned on whether a propagating photon is coupled to the dipole transition. Recently, deterministic entangling gates on single photons and single emitters [45,46,82] have been proposed with negatively charged quantum dots which have two independent dipole transitions and the initialization of this system usually takes a much longer time. For a  $\Lambda$ -type emitter, it could, in principle, be initialized to an arbitrary state determined by the state of an input photon, because a passive quantum swapping exchanges the states of an input photon and the emitter. Moreover, arbitrary single-qubit rotations on both a stationary emitter and a polarized input photon are easily achievable by faithful optical control and passive linear-optical elements. Furthermore, when the  $\Lambda$ -type atom is initially in

the excited state  $|E\rangle$ , the circular-dipole transitions generate a maximally entangled state between the atom and a photon encoded in the propagating modes [66].

Our MQI combines the advantages of chiral quantum optics and  $\Lambda$ -type systems, and it has the following two important merits. (i) If an input photon is *resonantly* coupled to the dipole transitions, then the destructive interference of the incident and transmitted modes of the photon leads to a complete photon reflection accompanied by a ground-state flip of the atom, analogously to the one observed for the Sagnac interferometers [64]. However, (ii) if an input photon is *nonresonantly* coupled to the transitions, then it can be both reflected and transmitted with some nonzero probabilities. In particular, if the detuning  $\Delta$  is equal to  $(\pm\Gamma)$ , then the reflection and transmission probabilities are equal to each other. This generates a maximally entangled state between the atom and the photon. This entanglement can be transferred (via transmitted photons and using the SWAP gates) into the entanglement between two different quantum nodes of quantum repeater-based networks [87–90].

In summary, we have presented an effective atom-photon interface with a chiral waveguide. The tunable scattering process is exploited to design the MQI for quantum networks, such as quantum swapping and hybrid-entanglement generation between a single atom and a single-photon pulse, which then leads to direct layouts of quantum memory and the entanglement between different nodes. A high performance of this proposed MQI is within reach of the existing experimental capabilities. Moreover, both the fidelity and the efficiency of the MQI are robust to the potential imperfections originating from a finite bandwidth of a single photon and a finite effective coupling constant between the atom and a waveguide, which makes our proposal useful for realistic quantum networks.

## ACKNOWLEDGMENTS

This work was supported in part by the MURI Center for Dynamic Magneto-Optics via the Air Force Office of Scientific Research (AFOSR) (Grant No. FA9550-14-1-0040), the Army Research Office (ARO) (Grant No. 73315PH), the Asian Office of Aerospace Research and Development (AOARD) (Grant No. FA2386-18-1-4045), the Japan Science and Technology Agency (JST) (the ImPACT program and CREST Grant No. JPMJCR1676), the Japan Society for the Promotion of Science (JSPS) (JSPS-RFBR Grant No. 17-52-50023), the RIKEN-AIST Challenge Research Fund, and the John Templeton Foundation. T.L. thanks Yuran Zhang for helpful discussions. X.H. also acknowledges support by US ARO via Grant No. W911NF1710257. K.X. acknowledges the support of the National Key R&D Program of China (Grant No. 2017YFA0303703) and the “1000 Young Talent” program.

- [1] H. J. Kimble, The quantum internet, *Nature (London)* **453**, 1023 (2008).  
 [2] S.-B. Zheng, C.-P. Yang, and F. Nori, Arbitrary control of coherent dynamics for distant qubits in a quantum network, *Phys. Rev. A* **82**, 042327 (2010).

- [3] F.-G. Deng and G. L. Long, Secure direct communication with a quantum one-time pad, *Phys. Rev. A* **69**, 052319 (2004).  
 [4] J. I. Cirac, P. Zoller, H. J. Kimble, and H. Mabuchi, Quantum State Transfer and Entanglement Distribution among Distant Nodes in a Quantum Network, *Phys. Rev. Lett.* **78**, 3221 (1997).

- [5] S. Ritter, C. Nölleke, C. Hahn, A. Reiserer, A. Neuzner, M. Uphoff, M. Mücke, E. Figueroa, J. Bochmann, and G. Rempe, An elementary quantum network of single atoms in optical cavities, *Nature (London)* **484**, 195 (2012).
- [6] J.-W. Pan, Z.-B. Chen, C.-Y. Lu, H. Weinfurter, A. Zeilinger, and M. Żukowski, Multiphoton entanglement and interferometry, *Rev. Mod. Phys.* **84**, 777 (2012).
- [7] F.-G. Deng, B.-C. Ren, and X.-H. Li, Quantum hyperentanglement and its applications in quantum information processing, *Sci. Bull.* **62**, 46 (2017).
- [8] L. Li, Y. Dudin, and A. Kuzmich, Entanglement between light and an optical atomic excitation, *Nature (London)* **498**, 466 (2013).
- [9] Y. Hao, G. Lin, K. Xia, X. Lin, Y. Niu, and S. Gong, Quantum controlled-phase-flip gate between a flying optical photon and a Rydberg atomic ensemble, *Sci. Rep.* **5**, 10005 (2015).
- [10] P. Lodahl, S. Mahmoodian, and S. Stobbe, Interfacing single photons and single quantum dots with photonic nanostructures, *Rev. Mod. Phys.* **87**, 347 (2015).
- [11] A. Reiserer and G. Rempe, Cavity-based quantum networks with single atoms and optical photons, *Rev. Mod. Phys.* **87**, 1379 (2015).
- [12] Z.-L. Xiang, S. Ashhab, J. Q. You, and F. Nori, Hybrid quantum circuits: Superconducting circuits interacting with other quantum systems, *Rev. Mod. Phys.* **85**, 623 (2013).
- [13] A. Kuhn, M. Hennrich, and G. Rempe, Deterministic Single-Photon Source for Distributed Quantum Networking, *Phys. Rev. Lett.* **89**, 067901 (2002).
- [14] M. Keller, B. Lange, K. Hayasaka, W. Lange, and H. Walther, Continuous generation of single photons with controlled waveform in an ion-trap cavity system, *Nature (London)* **431**, 1075 (2004).
- [15] A. Holleczek, O. Barter, A. Rubenok, J. Dille, P. B. R. Nisbet-Jones, G. Langfahl-Klabes, G. D. Marshall, C. Sparrow, J. L. O'Brien, K. Poulios, A. Kuhn, and J. C. F. Matthews, Quantum Logic with Cavity Photons from Single Atoms, *Phys. Rev. Lett.* **117**, 023602 (2016).
- [16] S. Barik, A. Karasahin, C. Flower, T. Cai, H. Miyake, W. DeGottardi, M. Hafezi, and E. Waks, A topological quantum optics interface, *Science* **359**, 666 (2018).
- [17] L.-M. Duan and H. J. Kimble, Scalable Photonic Quantum Computation through Cavity-Assisted Interactions, *Phys. Rev. Lett.* **92**, 127902 (2004).
- [18] K. Koshino, S. Ishizaka, and Y. Nakamura, Deterministic photon-photon  $\sqrt{\text{SWAP}}$  gate using a  $\Lambda$  system, *Phys. Rev. A* **82**, 010301 (2010).
- [19] A. Reiserer, N. Kalb, G. Rempe, and S. Ritter, A quantum gate between a flying optical photon and a single trapped atom, *Nature (London)* **508**, 237 (2014).
- [20] T. Tiecke, J. D. Thompson, N. P. de Leon, L. Liu, V. Vuletić, and M. D. Lukin, Nanophotonic quantum phase switch with a single atom, *Nature (London)* **508**, 241 (2014).
- [21] W. Qin, X. Wang, A. Miranowicz, Z. Zhong, and F. Nori, Heralded quantum controlled-phase gates with dissipative dynamics in macroscopically distant resonators, *Phys. Rev. A* **96**, 012315 (2017).
- [22] B. Hacker, S. Welte, G. Rempe, and S. Ritter, A photon-photon quantum gate based on a single atom in an optical resonator, *Nature (London)* **536**, 193 (2016).
- [23] S. Sun, H. Kim, G. S. Solomon, and E. Waks, A quantum phase switch between a single solid-state spin and a photon, *Nat. Nanotechnol.* **11**, 539 (2016).
- [24] X. Maitre, E. Hagley, G. Nogues, C. Wunderlich, P. Goy, M. Brune, J. M. Raimond, and S. Haroche, Quantum Memory with a Single Photon in a Cavity, *Phys. Rev. Lett.* **79**, 769 (1997).
- [25] L. Zhou, Z. R. Gong, Y.-x. Liu, C. P. Sun, and F. Nori, Controllable Scattering of a Single Photon Inside a One-Dimensional Resonator Waveguide, *Phys. Rev. Lett.* **101**, 100501 (2008).
- [26] L. Zhou, L.-P. Yang, Y. Li, and C. P. Sun, Quantum Routing of Single Photons with a Cyclic Three-Level System, *Phys. Rev. Lett.* **111**, 103604 (2013).
- [27] J. Lu, L. Zhou, L.-M. Kuang, and F. Nori, Single-photon router: Coherent control of multichannel scattering for single photons with quantum interferences, *Phys. Rev. A* **89**, 013805 (2014).
- [28] S. Rosenblum, S. Parkins, and B. Dayan, Photon routing in cavity QED: Beyond the fundamental limit of photon blockade, *Phys. Rev. A* **84**, 033854 (2011).
- [29] C. Y. Hu, Spin-based single-photon transistor, dynamic random access memory, diodes, and routers in semiconductors, *Phys. Rev. B* **94**, 245307 (2016).
- [30] C. Cao, Y.-W. Duan, X. Chen, R. Zhang, T.-J. Wang, and C. Wang, Implementation of single-photon quantum routing and decoupling using a nitrogen-vacancy center and a whispering-gallery-mode resonator-waveguide system, *Opt. Express* **25**, 16931 (2017).
- [31] K. Xia, G. Lu, G. Lin, Y. Cheng, Y. Niu, S. Gong, and J. Twamley, Reversible nonmagnetic single-photon isolation using unbalanced quantum coupling, *Phys. Rev. A* **90**, 043802 (2014).
- [32] I. Shomroni, S. Rosenblum, Y. Lovsky, O. Bechler, G. Guendelman, and B. Dayan, All-optical routing of single photons by a one-atom switch controlled by a single photon, *Science* **345**, 903 (2014).
- [33] T. Aoki, A. S. Parkins, D. J. Alton, C. A. Regal, B. Dayan, E. Ostby, K. J. Vahala, and H. J. Kimble, Efficient Routing of Single Photons by One Atom and a Microtoroidal Cavity, *Phys. Rev. Lett.* **102**, 083601 (2009).
- [34] X. Gu, A. F. Kockum, A. Miranowicz, Y.-x. Liu, and F. Nori, Microwave photonics with superconducting quantum circuits, *Phys. Rep.* **718-719**, 1 (2017).
- [35] J.-T. Shen and S. Fan, Coherent photon transport from spontaneous emission in one-dimensional waveguides, *Opt. Lett.* **30**, 2001 (2005).
- [36] M. Arcari, I. Söllner, A. Javadi, S. Lindskov Hansen, S. Mahmoodian, J. Liu, H. Thyrestrup, E. H. Lee, J. D. Song, S. Stobbe, and P. Lodahl, Near-Unity Coupling Efficiency of a Quantum Emitter to a Photonic Crystal Waveguide, *Phys. Rev. Lett.* **113**, 093603 (2014).
- [37] P. Lodahl, S. Mahmoodian, S. Stobbe, A. Rauschenbeutel, P. Schneeweiss, J. Volz, H. Pichler, and P. Zoller, Chiral quantum optics, *Nature (London)* **541**, 473 (2017).
- [38] P.-O. Guimond, H. Pichler, A. Rauschenbeutel, and P. Zoller, Chiral quantum optics with V-level atoms and coherent quantum feedback, *Phys. Rev. A* **94**, 033829 (2016).
- [39] H. Pichler, T. Ramos, A. J. Daley, and P. Zoller, Quantum optics of chiral spin networks, *Phys. Rev. A* **91**, 042116 (2015).
- [40] K. Y. Bliokh and F. Nori, Characterizing optical chirality, *Phys. Rev. A* **83**, 021803 (2011).

- [41] K. Y. Bliokh, A. Y. Bekshaev, and F. Nori, Extraordinary momentum and spin in evanescent waves, *Nat. Commun.* **5**, 3300 (2014).
- [42] K. Y. Bliokh, D. Smirnova, and F. Nori, Quantum spin hall effect of light, *Science* **348**, 1448 (2015).
- [43] K. Y. Bliokh, F. Rodríguez-Fortuño, F. Nori, and A. V. Zayats, Spin-orbit interactions of light, *Nat. Photonics* **9**, 796 (2015).
- [44] K. Y. Bliokh and F. Nori, Transverse and longitudinal angular momenta of light, *Phys. Rep.* **592**, 1 (2015).
- [45] A. B. Young, A. C. T. Thijssen, D. M. Beggs, P. Androvitsaneas, L. Kuipers, J. G. Rarity, S. Hughes, and R. Oulton, Polarization Engineering in Photonic Crystal Waveguides for Spin-Photon Entanglers, *Phys. Rev. Lett.* **115**, 153901 (2015).
- [46] I. Söllner, S. Mahmoodian, S. L. Hansen, L. Midolo, A. Javadi, G. Kiršanskė, T. Pregolato, H. El-Ella, E. H. Lee, J. D. Song, S. Stobbe, and P. Lodahl, Deterministic photon-emitter coupling in chiral photonic circuits, *Nat. Nanotechnol.* **10**, 775 (2015).
- [47] G.-Z. Song, E. Munro, W. Nie, F.-G. Deng, G.-J. Yang, and L.-C. Kwek, Photon scattering by an atomic ensemble coupled to a one-dimensional nanophotonic waveguide, *Phys. Rev. A* **96**, 043872 (2017).
- [48] L. Zhou, H. Dong, Y.-X. Liu, C. P. Sun, and F. Nori, Quantum supercavity with atomic mirrors, *Phys. Rev. A* **78**, 063827 (2008).
- [49] Y. Chang, Z. R. Gong, and C. P. Sun, Multiatomic mirror for perfect reflection of single photons in a wide band of frequency, *Phys. Rev. A* **83**, 013825 (2011).
- [50] D. E. Chang, L. Jiang, A. V. Gorshkov, and H. J. Kimble, Cavity QED with atomic mirrors, *New J. Phys.* **14**, 063003 (2012).
- [51] F. Fratini, E. Mascarenhas, L. Safari, J.-P. Poizat, D. Valente, A. Auffèves, D. Gerace, and M. F. Santos, Fabry-Perot Interferometer with Quantum Mirrors: Nonlinear Light Transport and Rectification, *Phys. Rev. Lett.* **113**, 243601 (2014).
- [52] N. V. Corzo, B. Gouraud, A. Chandra, A. Goban, A. S. Sheremet, D. V. Kupriyanov, and J. Laurat, Large Bragg Reflection from One-Dimensional Chains of Trapped Atoms Near a Nanoscale Waveguide, *Phys. Rev. Lett.* **117**, 133603 (2016).
- [53] D. E. Chang, A. S. Sørensen, E. A. Demler, and M. D. Lukin, A single-photon transistor using nanoscale surface plasmons, *Nat. Phys.* **3**, 807 (2007).
- [54] D. Witthaut and A. S. Sørensen, Photon scattering by a three-level emitter in a one-dimensional waveguide, *New J. Phys.* **12**, 043052 (2010).
- [55] E. Sánchez-Burillo, L. Martín-Moreno, D. Zueco, and J. J. García-Ripoll, One- and two-photon scattering from generalized V-type atoms, *Phys. Rev. A* **94**, 053857 (2016).
- [56] H. Zheng, D. J. Gauthier, and H. U. Baranger, Waveguide-QED-Based Photonic Quantum Computation, *Phys. Rev. Lett.* **111**, 090502 (2013).
- [57] Y. Li, L. Aolita, D. E. Chang, and L. C. Kwek, Robust-Fidelity Atom-Photon Entangling Gates in the Weak-Coupling Regime, *Phys. Rev. Lett.* **109**, 160504 (2012).
- [58] H. Zheng, D. J. Gauthier, and H. U. Baranger, Strongly correlated photons generated by coupling a three- or four-level system to a waveguide, *Phys. Rev. A* **85**, 043832 (2012).
- [59] F. Le Kien and A. Rauschenbeutel, Nanofiber-based all-optical switches, *Phys. Rev. A* **93**, 013849 (2016).
- [60] N. C. Harris, D. Bunandar, M. Pant, G. R. Steinbrecher, J. Mower, M. Prabhu, T. Baehr-Jones, M. Hochberg, and D. Englund, Large-scale quantum photonic circuits in silicon, *Nanophotonics* **5**, 456 (2016).
- [61] C. Sayrin, C. Junge, R. Mitsch, B. Albrecht, D. O'Shea, P. Schneeweiss, J. Volz, and A. Rauschenbeutel, Nanophotonic Optical Isolator Controlled by the Internal State of Cold Atoms, *Phys. Rev. X* **5**, 041036 (2015).
- [62] T. S. Tsoi and C. K. Law, Single-photon scattering on  $\Lambda$ -type three-level atoms in a one-dimensional waveguide, *Phys. Rev. A* **80**, 033823 (2009).
- [63] F. Ciccarello, D. E. Browne, L. C. Kwek, H. Schomerus, M. Zarcone, and S. Bose, Quasideterministic realization of a universal quantum gate in a single scattering process, *Phys. Rev. A* **85**, 050305 (2012).
- [64] M. Bradford and J.-T. Shen, Single-photon frequency conversion by exploiting quantum interference, *Phys. Rev. A* **85**, 043814 (2012).
- [65] I. Buluta, S. Ashhab, and F. Nori, Natural and artificial atoms for quantum computation, *Rep. Prog. Phys.* **74**, 104401 (2011).
- [66] B. Le Feber, N. Rotenberg, and L. Kuipers, Nanophotonic control of circular dipole emission, *Nat. Commun.* **6**, 6695 (2015).
- [67] H. J. Carmichael, *Statistical Methods in Quantum Optics 1: Master Equations and Fokker-Planck Equations* (Springer, New York, 1999).
- [68] M. B. Plenio and P. L. Knight, The quantum-jump approach to dissipative dynamics in quantum optics, *Rev. Mod. Phys.* **70**, 101 (1998).
- [69] E. Togan, Y. Chu, A. S. Trifonov, L. Jiang, J. Maze, L. Childress, M. V. G. Dutt, A. S. Sorensen, P. R. Hemmer, A. S. Zibrov, and M. D. Lukin, Quantum entanglement between an optical photon and a solid-state spin qubit, *Nature (London)* **466**, 730 (2010).
- [70] M. A. Nielsen, A simple formula for the average gate fidelity of a quantum dynamical operation, *Phys. Lett. A* **303**, 249 (2002).
- [71] X. Rong, J. Geng, F. Shi, Y. Liu, K. Xu, W. Ma, F. Kong, Z. Jiang, Y. Wu, and J. Du, Experimental fault-tolerant universal quantum gates with solid-state spins under ambient conditions, *Nat. Commun.* **6**, 8748 (2015).
- [72] M. A. Hall, J. B. Altepeter, and P. Kumar, Ultrafast Switching of Photonic Entanglement, *Phys. Rev. Lett.* **106**, 053901 (2011).
- [73] R. Takei and T. Mizumoto, Design and simulation of silicon waveguide optical circulator employing nonreciprocal phase shift, *Jpn. J. Appl. Phys.* **49**, 052203 (2010).
- [74] I. Aharonovich, S. Castelletto, D. Simpson, C. Su, A. Greentree, and S. Praver, Diamond-based single-photon emitters, *Rep. Prog. Phys.* **74**, 076501 (2011).
- [75] Y. Shen, T. M. Sweeney, and H. Wang, Zero-phonon linewidth of single nitrogen vacancy centers in diamond nanocrystals, *Phys. Rev. B* **77**, 033201 (2008).
- [76] C. Matthesen, A. N. Vamivakas, and M. Atatüre, Subnatural Linewidth Single Photons from a Quantum Dot, *Phys. Rev. Lett.* **108**, 093602 (2012).
- [77] D. D. B. Rao, S. Yang, and J. Wrachtrup, Generation of entangled photon strings using NV centers in diamond, *Phys. Rev. B* **92**, 081301(R) (2015).
- [78] H. Kosaka and N. Niikura, Entangled Absorption of a Single Photon with a Single Spin in Diamond, *Phys. Rev. Lett.* **114**, 053603 (2015).
- [79] P.-B. Li, Z.-L. Xiang, P. Rabl, and F. Nori, Hybrid Quantum Device with Nitrogen-Vacancy Centers in Diamond Coupled to Carbon Nanotubes, *Phys. Rev. Lett.* **117**, 015502 (2016).

- [80] T. G. Tiecke, K. P. Nayak, J. D. Thompson, T. Peyronel, N. P. De Leon, V. Vuletić, and M. D. Lukin, Efficient fiber-optical interface for nanophotonic devices, *Optica* **2**, 70 (2015).
- [81] M. J. Burek, C. Meuwly, R. E. Evans, M. K. Bhaskar, A. Sipahigil, S. Meesala, B. Machielse, D. D. Sukachev, C. T. Nguyen, J. L. Pacheco, E. Bielejec, M. D. Lukin, and M. Lončar, Fiber-Coupled Diamond Quantum Nanophotonic Interface, *Phys. Rev. Appl.* **8**, 024026 (2017).
- [82] S. Mahmoodian, P. Lodahl, and A. S. Sørensen, Quantum Networks with Chiral-Light-Matter Interaction in Waveguides, *Phys. Rev. Lett.* **117**, 240501 (2016).
- [83] S. Mahmoodian, K. Prindal-Nielsen, I. Söllner, S. Stobbe, and P. Lodahl, Engineering chiral light-matter interaction in photonic crystal waveguides with slow light, *Opt. Mater. Express* **7**, 43 (2017).
- [84] M. K. Bhaskar, D. D. Sukachev, A. Sipahigil, R. E. Evans, M. J. Burek, C. T. Nguyen, L. J. Rogers, P. Siyushev, M. H. Metsch, H. Park, F. Jelezko, M. Lončar, and M. D. Lukin, Quantum Nonlinear Optics with a Germanium-Vacancy Color Center in a Nanoscale Diamond Waveguide, *Phys. Rev. Lett.* **118**, 223603 (2017).
- [85] D. Riedel, I. Söllner, B. J. Shields, S. Starosielec, P. Appel, E. Neu, P. Maletinsky, and R. J. Warburton, Deterministic Enhancement of Coherent Photon Generation from a Nitrogen-Vacancy Center in Ultrapure Diamond, *Phys. Rev. X* **7**, 031040 (2017).
- [86] J. Riedrich-Möller, C. Arend, C. Pauly, F. Mücklich, M. Fischer, S. Gsell, M. Schreck, and C. Becher, Deterministic coupling of a single silicon-vacancy color center to a photonic crystal cavity in diamond, *Nano Lett.* **14**, 5281 (2014).
- [87] W. Dür, H.-J. Briegel, J. I Cirac, and P. Zoller, Quantum repeaters based on entanglement purification, *Phys. Rev. A* **59**, 169 (1999).
- [88] L. Jiang, J. M. Taylor, K. Nemoto, W. J. Munro, R. Van Meter, and M. D. Lukin, Quantum repeater with encoding, *Phys. Rev. A* **79**, 032325 (2009).
- [89] Y.-B. Sheng, L. Zhou, and G.-L. Long, Hybrid entanglement purification for quantum repeaters, *Phys. Rev. A* **88**, 022302 (2013).
- [90] W. J. Munro, A. M. Stephens, S. J. Devitt, K. A. Harrison, and K. Nemoto, Quantum communication without the necessity of quantum memories, *Nat. Photonics* **6**, 777 (2012).